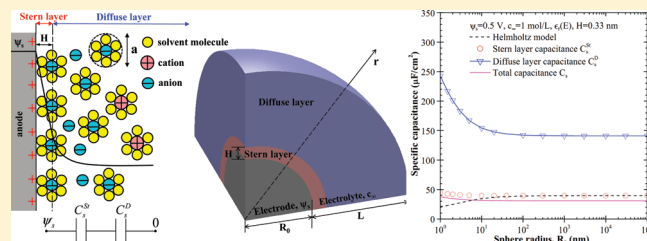


Accurate Simulations of Electric Double Layer Capacitance of Ultramicroelectrodes

Hainan Wang and Laurent Pilon*

Mechanical and Aerospace Engineering Department, Henry Samueli School of Engineering and Applied Science, University of California, Los Angeles, 420 Westwood Plaza, Los Angeles, California 90095, United States

ABSTRACT: This paper aims to develop rigorous and accurate numerical tools for simulating electric double layers formed near ultramicroelectrodes. It also aims to assess the validity of existing models and to identify the dominant physical phenomena that must be accounted for. The electric double layer capacitance was numerically predicted for spherical ultramicroelectrodes of various radii in aqueous electrolyte. The model accounted for the Stern and diffuse layers, the finite size of ions, and the dependency of the electrolyte dielectric permittivity on the local electric field. This study reveals that models reported in the literature suffer from severe limitations. First, it demonstrates that the electrolyte field-dependent dielectric permittivity significantly affects the predicted Stern layer and total specific capacitances and must be accounted for. The finite ion size and the Stern layer also need to be considered in simulating electric double layers under high concentrations and surface potential. This study also establishes that the Helmholtz model predicts the Stern layer capacitance for all electrode radii if the electrolyte permittivity is assumed to be constant. However, it underestimates the Stern layer capacitance for sphere radii less than 40 nm when accounting for field-dependent permittivity. The electrode curvature was found to have negligible effect on the predicted specific capacitance for sphere radii larger than 40 nm. Then, the latter is equal to that of planar electrodes. Results of this study can be used to design electrodes for electrochemical sensors and electrical energy storage.



that the electrolyte field-dependent dielectric permittivity significantly affects the predicted Stern layer and total specific capacitances and must be accounted for. The finite ion size and the Stern layer also need to be considered in simulating electric double layers under high concentrations and surface potential. This study also establishes that the Helmholtz model predicts the Stern layer capacitance for all electrode radii if the electrolyte permittivity is assumed to be constant. However, it underestimates the Stern layer capacitance for sphere radii less than 40 nm when accounting for field-dependent permittivity. The electrode curvature was found to have negligible effect on the predicted specific capacitance for sphere radii larger than 40 nm. Then, the latter is equal to that of planar electrodes. Results of this study can be used to design electrodes for electrochemical sensors and electrical energy storage.

1. INTRODUCTION

Microelectrodes and ultramicroelectrodes (UMEs) have been the subjects of intense studies in electrochemical sensing^{1–9} and in electrical energy storage and conversion.^{10–21} Microelectrodes and ultramicroelectrodes refer to electrodes with characteristic sizes less than 25 μm .^{3–6} These electrodes have been used extensively in different scanning probe microscopy techniques.^{22–28} For example, scanning electrochemical potential microscopy (SECPM) was developed to directly measure the equilibrium electric potential profile in the electric double layer forming near electrode surfaces.^{24–28} It also provides information on the local charge distribution and electric field in the electrolyte. The size and geometry of UMEs are critical parameters determining the spatial and temporal resolutions of the measurements.^{22–28}

Moreover, electrodes with nanostructures and tailored morphology hold great promise to enhance the energy and power densities of electrical energy storage devices.^{10–21} For example, Pech et al.²⁹ synthesized onion-like carbon spheres 6–7 nm in diameter and used them to synthesize electrodes for electric double layer capacitors (EDLCs) using electrophoretic deposition. The volumetric power density of their EDLC devices was comparable to that of conventional electrolytic capacitors, while the volumetric energy density was 1 order of magnitude larger.²⁹ This was attributed to the electrode's fully accessible surface area.²⁹

In all the above-mentioned applications, understanding the electric double layer structure is of great importance for the rational and optimum design of the electrode morphology.^{15–18,25–28}

For this purpose, numerical simulations can facilitate the design of electrodes in a more systematic and efficient way than a trial-and-error approach. They can also account for various and complex phenomena and identify the dominant processes governing the capacitance behavior of the electrode. This paper aims to develop rigorous and accurate numerical tools for simulating electric double layers formed near ultramicroelectrodes. It also assesses the validity of analytical expressions for the capacitance of ultramicroelectrodes.

2. BACKGROUND

2.1. Helmholtz Model. Helmholtz³⁰ was the first to propose the concept of the electric double layer. He realized that charged electrodes immersed in electrolyte solutions will repel the cations while attracting counterions to their surfaces. The two compact layers of charges formed at the electrode/electrolyte interfaces were called the “electric double layer” (EDL). Figure 1a shows a schematic of the electric double layer structure formed at the anode surface as envisioned by Helmholtz.^{30–34} In the Helmholtz model, all the counterions were assumed to be adsorbed at the electrode surface.^{30–32} This structure is analogous to that of conventional dielectric capacitors with two

Received: May 13, 2011

Revised: July 7, 2011

Published: July 15, 2011

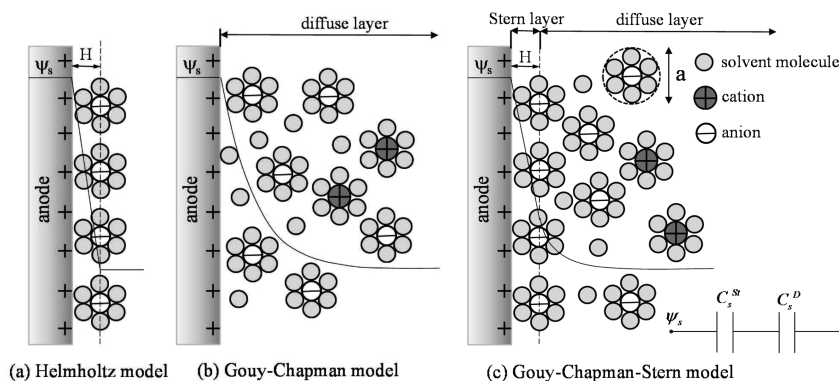


Figure 1. Schematics of the electric double layer structure showing the arrangement of solvated anions and cations near the electrode/electrolyte interface in the Stern layer and the diffuse layer. (a) Helmholtz model, (b) Gouy–Chapman model, and (c) Gouy–Chapman–Stern model.

planar electrodes separated by a distance H .^{30–32} Therefore, the capacitance per unit surface area (or specific capacitance) of the Helmholtz double layer denoted by C_s^H and expressed in F/m^2 is given by^{35–39}

$$C_s^H = \begin{cases} \frac{\epsilon_0 \epsilon_r}{H} & \text{for planar electrode} & (1a) \\ \frac{\epsilon_0 \epsilon_r}{R_0 \log(1 + H/R_0)} & \text{for cylindrical electrode of radius } R_0 & (1b) \\ \frac{\epsilon_0 \epsilon_r}{H} \left(1 + \frac{H}{R_0}\right) & \text{for spherical electrode of radius } R_0 & (1c) \end{cases}$$

where ϵ_0 and ϵ_r are the free space permittivity and the relative permittivity of the electrolyte solutions, respectively. The thickness H of the Helmholtz double layer can be approximated as the radius of solvated ions.^{31,33,34} Note that eqs 1b and 1c reduce to the asymptotic expression given by eq 1a when the electrode radius is large enough, i.e., $R_0 \gg H$.

2.2. Gouy–Chapman Model. Gouy⁴⁰ and Chapman⁴¹ developed an electric double layer model accounting for the fact that the ions are mobile in the electrolyte solutions and are driven by the coupled influences of diffusion and electrostatic forces.^{31,32,34} This results in the so-called “diffuse layer” shown in Figure 1b. In this model, the ions are treated as point charges and the equilibrium concentration c_i of ion species i is given by the Boltzmann distribution as^{31–34,42–44}

$$c_i = c_{i\infty} \exp\left(\frac{-z_i e \psi}{k_B T}\right) \quad (2)$$

where z_i and $c_{i\infty}$ are the valency and bulk molar concentration of ion species i , respectively. The absolute temperature is denoted by T , e is the elementary charge, and k_B is the Boltzmann constant ($k_B = 1.381 \times 10^{-23} \text{ m}^2 \text{ kg K}^{-1} \text{ s}^{-2}$). In the Gouy–Chapman model, the local electric potential ψ in the diffuse layer is determined by the Poisson–Boltzmann (PB) equation assuming constant electrolyte permittivity.^{31–34,42–44} For binary symmetric electrolytes, $z_1 = -z_2 = z$ and $c_{1\infty} = c_{2\infty} = c_\infty$. Then, the PB equation is expressed as^{31–34,42–44}

$$\nabla \cdot (\epsilon_0 \epsilon_r \nabla \psi) = 2zeN_A c_\infty \sinh\left(\frac{ze\psi}{k_B T}\right) \quad (3)$$

where N_A is the Avogadro’s number ($N_A = 6.022 \times 10^{23} \text{ mol}^{-1}$).

For planar electrodes and constant electrolyte properties, the exact solution of eq 3 exists subject to the following boundary conditions: (i) $\psi(0) = \psi_D$ and (ii) $\psi(\infty) = 0$. Then, the specific capacitance corresponding to the diffuse layer C_s^D is given

by^{31–34,42–44}

$$C_s^D = \frac{q_s}{\psi_D} = \frac{4zeN_A c_\infty \lambda_D}{\psi_D} \sinh\left(\frac{ze\psi_D}{2k_B T}\right) \quad (4)$$

where q_s is the surface charge density and λ_D is the Debye length for symmetric electrolytes defined as $\lambda_D = [(\epsilon_0 \epsilon_r k_B T / 2e^2 z^2 N_A c_\infty)^{1/2}]$.^{31–34,42–44}

For spherical electrodes, the exact solution of eq 3 exists provided that the Debye–Hückel approximation requiring $z_i e \psi / k_B T \ll 1$ is satisfied.^{34,42–44} Then, the diffuse layer specific capacitance is given by^{34,42–44}

$$C_s^D = \frac{\epsilon_0 \epsilon_r}{\lambda_D} \left(1 + \frac{\lambda_D}{R_0}\right) \quad (5)$$

Equations 4 and 5 reduce to the same asymptotic expression of $C_s^D = \epsilon_0 \epsilon_r / \lambda_D$ when the Debye–Hückel approximation and the thin double layer approximation assuming $\lambda_D / R_0 \ll 1$ are satisfied.^{34,42–44}

2.3. Gouy–Chapman–Stern Model. Stern⁴⁵ combined the Helmholtz model and the Gouy–Chapman model and described the electric double layer as two layers (Figure 1c), namely, (i) the Stern layer (or Helmholtz layer), referring to the compact layer of immobile ions strongly adsorbed to the electrode surface, and (ii) the diffuse layer where the ions are mobile and the Gouy–Chapman model (eq 3) applies.^{31–34,42–44} Note that there are no free charges within the Stern layer.^{31,32,34,42}

The total electric double layer capacitance consists of the Stern layer and diffuse layer capacitances in series.^{31,32,42,43} Mathematically, the Gouy–Chapman–Stern (GCS) model for symmetric electrolytes is expressed as^{42,46,47}

$$\nabla \cdot (\epsilon_0 \epsilon_r \nabla \psi) = \begin{cases} 0 & \text{in the Stern layer} & (6a) \\ 2zeN_A c_\infty \sinh\left(\frac{ze\psi}{k_B T}\right) & \text{in the diffuse layer} & (6b) \end{cases}$$

2.4. Effect of Finite Size of Ions. The point-charge assumption associated with the Poisson–Boltzmann equation (eqs 3 and 6b) is only valid for very low ion concentration c_∞ and low electric potential.^{31,32,43} In reality, the ions have finite size and thus a maximum ion concentration c_{\max} exists corresponding to the closed packing of ions. It is given by $c_{\max} = 1/(N_A a^3)$ corresponding to simple cubic packing of ions with effective diameter a .^{48,49} Therefore, the ion concentration given by the Boltzmann distribution (eq 2) should not exceed c_{\max} . This

corresponds to a maximum surface potential ψ_{\max} given by^{48,49}

$$\psi_{\max} = -\frac{k_{\text{B}}T}{ze} \log(N_{\text{A}}a^3c_{\infty}) \quad (7)$$

The magnitude of the local electric potential $|\psi|$ in the diffuse layer should not exceed ψ_{\max} for the Gouy–Chapman and Gouy–Chapman–Stern models (eqs 3 and 6b) to be valid. For example, $\psi_{\max} = 0.04$ V for the typical values of $T = 298$ K, $z = 1$, $c_{\infty} = 1$ mol/L, and $a = 0.66$ nm.^{37–39,47}

Numerous studies have been reported in the literature to account for the effect of finite ion size in the electrolyte solution.^{49–53} Among them, the modified Poisson–Boltzmann (MPB) models based on the local-density and mean-field approximations are relatively convenient both mathematically and numerically.^{49–53} Among different MPB models, Bikerman's model is the simplest for symmetric electrolytes and is expressed as^{48,49,53–55}

$$\nabla \cdot (\epsilon_0 \epsilon_r \nabla \psi) = \frac{2zeN_{\text{A}}c_{\infty} \sinh\left(\frac{ze\psi}{k_{\text{B}}T}\right)}{1 + 2\nu \sinh^2\left(\frac{ze\psi}{2k_{\text{B}}T}\right)} \quad (8)$$

where the packing parameter is defined as $\nu = 2a^3N_{\text{A}}c_{\infty} = 2c_{\infty}/c_{\text{max}}$.^{48,49,53–55} From here on, the term “MPB model” will be used to refer to eq 8. When $\nu = 0$, the MPB model reduces to the Gouy–Chapman model given by eq 3. For planar electrodes and constant electrolyte properties, the surface charge density and diffuse layer specific capacitance are given by^{48,49,52}

$$C_{\text{s}}^{\text{D}} = \frac{q_{\text{s}}}{\psi_{\text{D}}} = \frac{2zeN_{\text{A}}c_{\infty}\lambda_{\text{D}}}{\psi_{\text{D}}} \sqrt{\frac{2}{\nu} \log\left[1 + 2\nu \sinh^2\left(\frac{ze\psi_{\text{D}}}{2k_{\text{B}}T}\right)\right]} \quad (9)$$

Note that when $\psi_{\text{D}} = 0$, eq 9 predicts an extremum for the diffuse layer capacitance, i.e., $C_{\text{s}}^{\text{D}} = \epsilon_0 \epsilon_r / \lambda_{\text{D}}$. This capacitance could be either a maximum or a minimum value depending on the packing parameter ν as discussed in refs 48, 49, 52, and 53.

2.5. Simulations of Electric Double Layer near Ultramicroelectrodes. The above-discussed models have been used extensively to investigate the electric double layer near ultramicroelectrodes despite their inherent limitations. Huang et al.^{37–39} used the Helmholtz model (eqs 1a–1c) to predict the specific capacitance of EDLCs based on single spherical and cylindrical electrode carbon particles as well as single cylindrical pores. Their models predicted that the total specific capacitance decreases with increasing electrode radius larger than 2 nm. However, the electrolyte permittivity was used as an empirical parameter to match the specific capacitance predicted by eqs 1a–1c with experimental data.^{37–39}

Compton and co-workers^{56,57} investigated the effect of the electrode curvature on the diffuse layer formed at the surface of single hemispherical and cylindrical nanoelectrodes. The authors solved the Gouy–Chapman model (eq 3) numerically for electrode radii ranging from 2 nm to 100 μm . The surface electric potential ψ_{s} was less than 0.25 V, and the electrolyte concentration c_{∞} was less than 0.1 mol/L. They observed a significantly enhanced surface charge density for a sphere radius less than 50 nm and attributed this phenomenon to the “non-classical behavior” caused by the large electrode curvature.^{56,57}

However, it should be noted that this trend could be readily predicted by the exact solution given by eq 5. Moreover, the Gouy–Chapman model used in refs 56 and 57 is limited to very low ion concentrations and electric potentials.

Huang et al.⁴⁷ used the Gouy–Chapman–Stern model to investigate the effects of the shape and geometry of a single nanopore on the specific capacitance. They explored “slit” and cylindrical pores with diameters ranging from 2 to 16 nm. The dielectric permittivity $\epsilon_r = 9.73$ was imposed in the Stern layer based on the values previously fitted in refs 37,38, while $\epsilon_r = 36$ in the diffuse layer.⁴⁷ The electrolyte concentration was $c_{\infty} = 1.0$ mol/L, and the electrode surface potential was $\psi_{\text{s}} = 1$ V. However, the Gouy–Chapman–Stern model breaks down for such a concentration and potential as ions can no longer be treated as point charges.^{48,49}

Hamou et al.^{27,28} numerically investigated the electric potential profile near the probe apex in SECPMs by simulating planar and spherical electrodes. Their model accounted for both the Stern layer and the finite size of ions and solved the MPB model given by eq 8. The electrolyte concentration c_{∞} ranged from 10^{-5} to 10^{-2} mol/L, while the surface potential ψ_{s} varied from 0.2 to 0.4 V.^{27,28} The authors investigated the effects of the shape and size of the probe on the electric potential profile in the electrolyte. They found that a sharper apex resulted in (i) higher electric field and surface charge density at the probe vertex and (ii) better resolution of the electric potential in the lateral direction.^{27,28}

In nearly all the above-mentioned references, the electrolyte dielectric permittivity was assumed to be constant and sometimes was treated as a fitting parameter. However, the relative permittivity ϵ_r of polar electrolytes is known to significantly decrease as the electric field increases.^{58–65} In fact, the individual electrolyte molecules become highly oriented under a large electric field. Therefore, further orientation of the molecules can hardly provide more polarization and the relative permittivity decreases.^{60–62} Booth derived the following model to account for the dependency of electrolyte dielectric permittivity on the local electric field larger than 10^7 V/m:^{58–60}

$$\epsilon_r(E) = n^2 + (\epsilon_r(0) - n^2) \frac{3}{\beta E} \left[\coth(\beta E) - \frac{1}{\beta E} \right] \quad (10a)$$

while ϵ_r can be treated as constant for $E < 10^7$ V/m

$$\epsilon_r(E) = \epsilon_r(0) \quad (10b)$$

Here, $E = |-\nabla\psi|$ is the norm of the local electrical field vector, $\epsilon_r(0)$ is the relative permittivity at zero electric field, and n is the index of refraction of the electrolyte at zero electric field frequency. Results of molecular dynamics simulations for different electrolytes^{62–64} have verified that the Booth model accurately predicts the electrolyte permittivity for high electric fields up to 4 V/nm typically encountered in EDLCs.^{64,66} Moreover, the Booth model has been combined with the Poisson equation in refs 67–69 to investigate the repulsion between two charged planar surface electrodes due to hydration forces in aqueous electrolyte solutions. Hamou et al.²⁸ investigated the effect of field-dependent electrolyte permittivity using the Booth model in the simulations of SECPM. However, they did not observe significant changes in the dielectric permittivity and in electric potential profiles.²⁸

More recently, Wang et al.⁷⁰ utilized the MPB and Booth models to predict the specific capacitance of closely packed

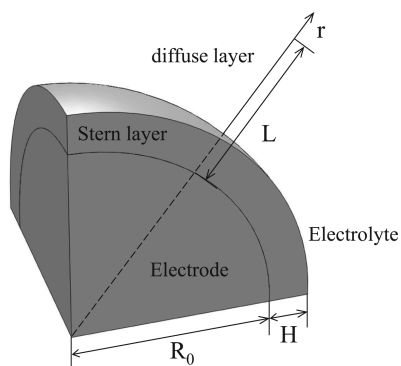


Figure 2. Schematic and coordinate system of the simulated computational domain consisting of the Stern layer and the diffuse layer. The problem is one-dimensional in spherical coordinates by virtue of symmetry.

monodispersed sphere arrays with different packing morphologies and sphere diameters. The numerical results established that the diffuse layer specific capacitance of the sphere arrays significantly decreased when the field-dependent electrolyte permittivity was accounted for.⁷⁰ However, the Stern layer capacitance was predicted using the Helmholtz model (eq 1a), rather than by simulating the complete electric double layer structure consisting of both the Stern and diffuse layers.

This paper aims to clarify the dominant physical phenomena that must be accounted for in simulating electric double layers formed near ultramicroelectrodes. It also assesses the validity of the Helmholtz model. An equilibrium model based on continuum theory was developed to predict the specific capacitance of a single spherical electrode particle with various radii. To the best of our knowledge, the present study is the first to simulate the electric double layer capacitance of ultramicroelectrodes by simultaneously accounting for (1) the Stern and diffuse layers, (2) the finite size of ions, and (3) field-dependent dielectric permittivity. Note that the double layer capacitances also significantly depend on surface electric potential,^{48,49} electrolyte concentration,^{52,53} and temperature (eq 8). This has been explored extensively in the literature and need not be repeated.

3. ANALYSIS

3.1. Schematics and Assumptions. Figure 2 shows the schematic of the computational domain simulated in the present study. A spherical electrode of radius R_0 was immersed in an electrolyte solution. The region of electrolyte solution consists of two layers corresponding to (1) a Stern layer of thickness H near the electrode surface and (2) a diffuse layer beyond. By virtue of symmetry, the problem was one-dimensional in the radial direction and was solved in spherical coordinates. The electric potential was prescribed as positive at the electrode surface and was zero far from the electrode surface. The length of the overall computational domain was specified to be $L = 80$ nm for all cases simulated. Increasing this length to 160 nm was found to have no effect on the predicted electric potential profile and on the specific capacitance.

To make the problem mathematically tractable, the following assumptions were made: (1) the electric potential and ion concentration were invariant with time (steady state) and reached their equilibrium states, (2) anions and cations had the

same and constant effective diameter^{48,49,71} independent of the electrolyte concentrations, (3) isothermal conditions prevailed throughout the electrode and electrolyte, (4) advection of the electrolyte was assumed to be negligible, and (5) the ions could only accumulate at the electrode surface and could not diffuse into the electrode particle; i.e., there was no ion insertion.

3.2. Governing Equation and Boundary Conditions. The local steady-state and equilibrium electric potential in the electrolyte solution denoted by $\psi(r)$ was computed by solving (i) eq 6a in the Stern layer and (ii) eq 8 in the diffuse layer. In addition, the coordinate transformation $R = r - R_0$ was used to simplify the governing equation to

$$\frac{1}{(R + R_0)^2} \frac{d}{dR} \left(\epsilon_0 \epsilon_r (R + R_0)^2 \frac{d\psi}{dR} \right) = \begin{cases} 0 & 0 \leq R \leq H & (11a) \\ \frac{2zeN_A c_\infty \sinh\left(\frac{ze\psi}{k_B T}\right)}{1 + 2\nu \sinh^2\left(\frac{ze\psi}{2k_B T}\right)} & R \geq H & (11b) \end{cases}$$

where R represents the distance from the electrode surface.

The associated boundary conditions were given by^{42,43}

$$\psi = \psi_s, \quad \text{at } R = 0 \quad (12a)$$

$$\psi|_{R=H^-} = \psi|_{R=H^+} \quad \text{and} \quad \epsilon_0 \epsilon_r \left. \frac{d\psi}{dR} \right|_{R=H^-} = \epsilon_0 \epsilon_r \left. \frac{d\psi}{dR} \right|_{R=H^+}, \quad \text{at } R = H \quad (12b)$$

$$\psi = 0, \quad \text{at } R = L \quad (12c)$$

Equation 12b states that the electric potential and displacement were continuous across the Stern/diffuse layers interface located at $R = H$.^{42,43} Cases when $H = 0$ in eqs 11a, 11b, and 12a–12c correspond to simulations without the Stern layer as performed in refs 48, 49, and 53–55.

3.3. Constitutive Relations. In order to solve eqs 11a, 11b, and 12a–12c, the electrolyte properties ϵ_r , z , c_∞ , and a along with the temperature T are needed. Here, the Booth model^{58–60} given by eqs 10a and 10b was used to account for the effects of the electric field on electrolyte relative permittivity. The present study focuses on aqueous binary symmetric electrolyte solution at room temperature ($T = 298$ K) characterized by the following properties: $\epsilon_r(0) = 78.5$,³² $n = 1.33$, and $\beta = 1.41 \times 10^{-8}$ V/m.^{67–69} The effective ion diameter was taken as $a = 0.66$ nm and the valency was $z = 1$ corresponding to solvated ions such as K^+ , OH^- , and Cl^- in aqueous solutions,⁷¹ for example. The electrolyte concentration was chosen as $c_\infty = 1.0$ mol/L corresponding to the typical values in EDLCs.

Finally, the Stern layer thickness H was approximated as the solvated ion radius; i.e., $H = a/2 = 0.33$ nm.^{31,33,34} In reality, the Stern layer thickness may be larger than the solvated ion radius due to the specific adsorption of solvent molecules or anions near the electrode surface.^{31–33,42,43} This is typically caused by non-electrostatic forces.^{31–33,42,43} A parametric study was also carried out for different values of Stern layer thickness, $H = 0, 0.33$, and 1.0 nm.

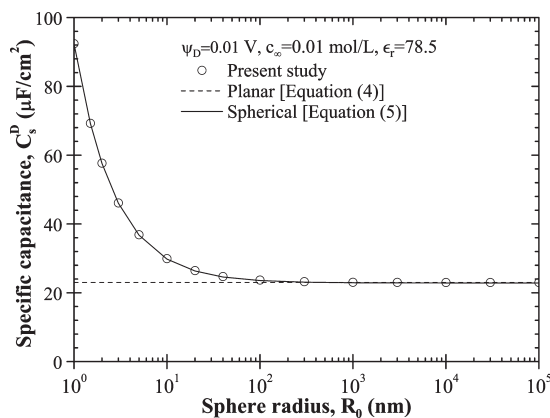


Figure 3. Predicted diffuse layer specific capacitance C_s^D obtained by numerically solving the Gouy–Chapman model (eq 3) assuming constant permittivity $\epsilon_r = 78.5$, $c_\infty = 0.01$ mol/L, and $\psi_D = 0.01$ V, along with the exact solutions for planar and spherical electrodes (eqs 4 and 5).

3.4. Method of Solution And Data Processing. Equations 11a and 11b were solved using the commercial finite element solver COMSOL 3.5a, along with the boundary conditions given by eqs 12a–12c. The model was solved for constant permittivity $\epsilon_r(0)$ or field-dependent permittivity $\epsilon_r(E)$ given by eqs 10a and 10b. The specific capacitances of the Stern and diffuse layers were computed by dividing the surface charge density^{34,72,73} $q_s(R) = \epsilon_0 \epsilon_r E(R)$ by their respective potential differences as^{31,32,43}

$$C_s^{\text{St}} = \frac{q_s(0)}{\psi_s - \psi_D} = \frac{\epsilon_0 \epsilon_r E(0)}{\psi_s - \psi_D} \quad \text{and} \quad (13)$$

$$C_s^D = \frac{q_s(H)}{\psi_D} = \frac{\epsilon_0 \epsilon_r E(H)}{\psi_D}$$

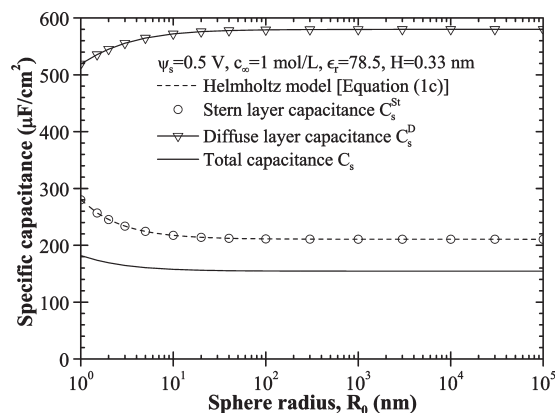
where $E(R) = |-\text{d}\psi/\text{d}R|(R)$ is the norm of the local electric field at location R while $\psi_D = \psi(H)$ is the electric potential computed at the Stern/diffuse layers interface. Then, the total specific capacitance C_s was calculated using the series formula as^{31,32,43}

$$\frac{1}{C_s} = \frac{1}{C_s^{\text{St}}} + \frac{1}{C_s^D} \quad (14)$$

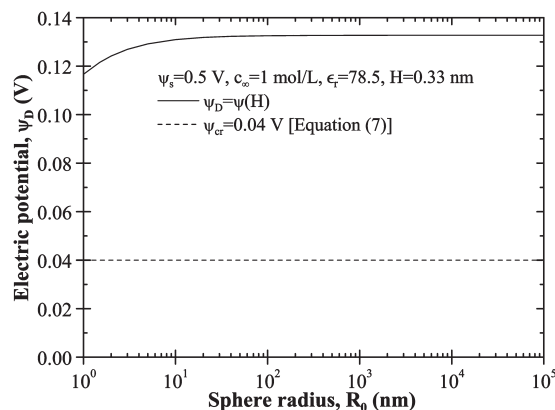
Numerical convergence was assessed based on the surface charge densities $q_s(R)$ at $R = 0$ and at $R = H$. The convergence criterion was chosen such that the maximum relative difference in both $q_s(0)$ and $q_s(H)$ was less than 1% when multiplying the total number of finite elements by 2. The total number of finite elements required to obtain a converged solution was less than 400 for all cases simulated in the present study.

3.5. Validation. The numerical tool was validated against (i) the exact solutions of the Gouy–Chapman model for planar electrodes (eq 4) and spherical electrodes (eq 5) for $\epsilon_r = 78.5$, $c_\infty = 0.01$ mol/L, and $\psi_D = 0.01$ V and (ii) the numerical results of the MPB model (eq 8) for planar electrodes reported in ref 48 for a wide range of packing parameter ν and dimensionless potential ($ze\psi_D/k_B T$). Excellent agreement was found in all cases considered.

Figure 3 shows the numerically predicted diffuse layer specific capacitance C_s^D as a function of sphere radius R_0 ranging from 1 nm to 100 μm . It was obtained by solving eqs 11a and 11b with $H = 0$ assuming constant permittivity $\epsilon_r = 78.5$, $c_\infty = 0.01$ mol/L, $a = 0.66$ nm (i.e., $\nu = 0.0035$), and $\psi_D = 0.01$ V. Figure 3 also



(a)



(b)

Figure 4. Predicted (a) Stern layer, diffuse layer, and total specific capacitances and (b) electric potential ψ_D at the diffuse layer boundary ($R = H = 0.33$ nm) obtained by numerically solving the Gouy–Chapman–Stern model (eqs 6a and 6b) assuming constant electrolyte permittivity $\epsilon_r = 78.5$, $c_\infty = 1$ mol/L, and $\psi_s = 0.5$ V.

shows the exact solutions for planar and spherical electrodes respectively given by eqs 4 and 5. The numerical predictions agreed quite well with the exact solutions for all values of electrode radius considered. It is evident that C_s^D decreased with increasing sphere radius. It also reached the asymptotic value of planar electrodes (eq 4) for sphere radii larger than 100 nm. This can be attributed to the fact that a smaller sphere radius results in a larger surface electric field⁷³ and thus larger surface charge and specific capacitance. These results are similar to the trend predicted numerically in refs 56 and 57 for spherical and cylindrical nanoelectrodes using $\psi_s = 0.25$ V and $c_\infty = 0.1$ mol/L. However, the observed trend is not due to “nonclassical behavior” but is based on classical continuum theory.

4. RESULTS AND DISCUSSION

4.1. Revisiting Gouy–Chapman–Stern Model. Figure 4a shows the numerically predicted Stern, diffuse, and total specific capacitances as a function of sphere radius R_0 ranging from 1 nm to 100 μm as well as the predictions using the Helmholtz model (eq 1c). Results were obtained by solving the Gouy–Chapman–Stern model (eqs 6a and 6b) assuming constant permittivity $\epsilon_r = 78.5$, $c_\infty = 1$ mol/L, $H = 0.33$ nm, and $\psi_s = 0.5$ V. The specific capacitances C_s^{St} , C_s^D , and C_s were computed using eqs 13 and 14. Figure 4a indicates that the predicted C_s^{St} decreased while C_s^D

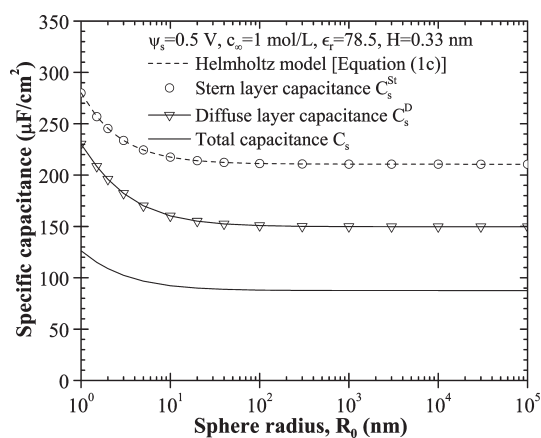


Figure 5. Predicted specific capacitances obtained by numerically solving the MPB model with Stern layer (eqs 11a, 11b, and 12a–12c) assuming constant electrolyte permittivity $\epsilon_r = 78.5$, $c_\infty = 1$ mol/L, and $\psi_s = 0.5$ V, while $H = a/2 = 0.33$ nm.

increased slightly with increasing sphere radius and reached a plateau for R_0 larger than 100 nm. In addition, the Stern layer specific capacitance C_s^{St} was much smaller than C_s^{D} . Thus, the total specific capacitance C_s was dominated by C_s^{St} according to eq 14.

Furthermore, Figure 4a indicates that the predictions of Helmholtz model (eq 1c) were identical to the computed Stern layer specific capacitance C_s^{St} . This can be attributed to the fact that, in both models, the electric potential is governed by Poisson's equation (eq 6a) assuming constant permittivity.^{35,36} Thus, the electric potential profile for planar electrodes is linear in both the Helmholtz model and the solution of the Gouy–Chapman–Stern model in the Stern layer.^{31–33,42,43} Consequently, both models predict the same specific capacitance, i.e., $C_s^{\text{H}} = C_s^{\text{St}}$. This also establishes that the Helmholtz model predicts the Stern layer capacitance rather than the total double layer capacitance as sometimes assumed in the literature for large electrolyte concentrations.^{37–39}

Figure 4b shows the predicted electric potential ψ_{D} at the diffuse layer boundary ($R = H = 0.33$ nm) as a function of sphere radius R_0 , as well as the maximum potential ψ_{max} given by eq 7 for $\epsilon_r = 78.5$, $c_\infty = 1$ mol/L, $H = 0.33$ nm, and $\psi_s = 0.5$ V. It indicates that the computed diffuse layer potential ψ_{D} was larger than the maximum potential $\psi_{\text{max}} = 0.04$ V for all values of sphere radius considered. Therefore, the Gouy–Chapman–Stern model (eqs 6a and 6b) was not valid for computing the diffuse layer capacitance C_s^{D} for such high concentration as the results do not satisfy the point-charge assumption.

4.2. Effect of Finite Size of Ions. Figure 5 shows the numerically predicted specific capacitances C_s^{St} , C_s^{D} , and C_s as a function of sphere radius R_0 obtained by solving the MPB model with Stern layer (eqs 11a, 11b, and 12a–12c). The model accounted for both the Stern layer and the finite ion size in the diffuse layer with effective ion diameter $a = 0.66$ nm. The other parameters were identical to those used to generate Figure 4a, i.e., $\epsilon_r = 78.5$, $c_\infty = 1$ mol/L, $H = a/2 = 0.33$ nm, and $\psi_s = 0.5$ V. Here again, the Stern layer specific capacitance C_s^{St} was identical to the predictions of (i) the Helmholtz model C_s^{H} (eq 1c) and (ii) of the Gouy–Chapman–Stern model (Figure 4a) for all values of the sphere radius. However, the predicted diffuse layer specific capacitance C_s^{D} decreased with increasing sphere radius in contrast to predictions from the Gouy–Chapman–Stern model shown in

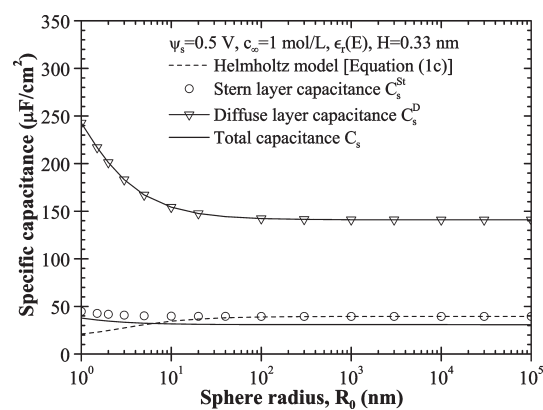


Figure 6. Predicted specific capacitances obtained by numerically solving the MPB model with Stern layer (eqs 11a, 11b, and 12a–12c) using field-dependent electrolyte permittivity (eqs 10a and 10b) with $c_\infty = 1$ mol/L, $\psi_s = 0.5$ V, and $H = a/2 = 0.66$ nm.

Figure 4a. Moreover, C_s^{D} was about 4 times smaller than that plotted in Figure 4a. Then, the total specific capacitance C_s was no longer dominated by the Stern layer specific capacitance and was about half that predicted by the Gouy–Chapman–Stern model (Figure 4a). These results demonstrate that the finite size of ions has a significant effect on the specific capacitance and must be accounted for in simulating the electric double layer for large electrolyte concentration and large electric potential. Here, again, the Helmholtz model cannot be used to predict the total specific capacitance.

4.3. Effect of Field-Dependent Dielectric Permittivity. Figure 6 shows the numerically predicted specific capacitances C_s^{St} , C_s^{D} , and C_s as a function of R_0 accounting for field-dependent permittivity. Results were obtained by solving the MPB model with Stern layer (eqs 11a, 11b, and 12a–12c) with $c_\infty = 1$ mol/L, $H = a/2 = 0.33$ nm, $\psi_s = 0.5$ V, and ϵ_r given by eqs 10a and 10b. It also shows the predictions by the Helmholtz model (eq 1c) using $\epsilon_r = \epsilon_r(E_s)$ based on the local electric field computed at the electrode surface $E_s = E(R=0)$.

Figure 6 indicates that the predicted Stern layer specific capacitance C_s^{St} using field-dependent permittivity $\epsilon_r(E_s)$ differed significantly from that obtained assuming constant permittivity (Figure 5). First, the numerical predictions assuming constant permittivity overestimated C_s^{St} by a factor of 4. Second, the predicted value of C_s^{St} was now in the range 40–45 $\mu\text{F}/\text{cm}^2$ and was about 4–5 times smaller than C_s^{D} . Third, the predicted Stern layer capacitance C_s^{St} was found to be nearly independent of the sphere radius. This can be attributed to the fact that a smaller sphere radius resulted in a larger surface electric field and thus smaller electrolyte permittivity. Overall, these competing effects balanced each other so that the surface charge density, given by $q_s = \epsilon_0 \epsilon_r(E_s) E_s$, and the specific capacitance C_s^{St} given by eq 13 did not change significantly as the sphere radius varied.

By contrast, the Helmholtz model predicted that the specific capacitance decreased with decreasing sphere radius less than 40 nm due to the significant decrease of electrolyte permittivity. In fact, the Helmholtz model underestimated the Stern layer capacitance for sphere radius less than 40 nm when accounting for field-dependent permittivity. Figure 6 also demonstrates that the predicted diffuse layer specific capacitance C_s^{D} using field-dependent permittivity $\epsilon_r(E)$ was nearly the same as the predictions assuming constant permittivity $\epsilon_r(0)$ shown in Figure 5.

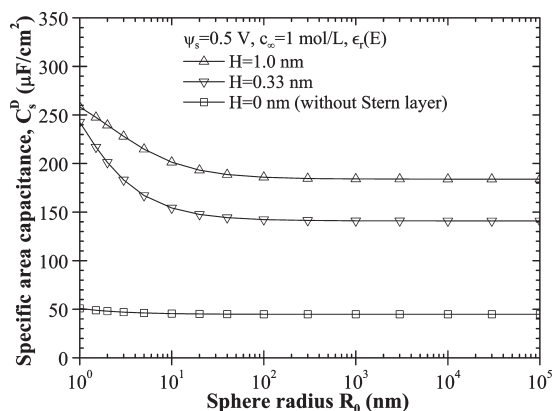


Figure 7. Predicted diffuse layer specific capacitance C_s^D obtained by numerically solving eqs 11a, 11b, and 12a–12c using field-dependent electrolyte permittivity (eqs 10a and 10b) for Stern layer thickness $H = 0$, 0.33, and 1.0 nm. Electrolyte concentration was set to be $c_\infty = 1$ mol/L and surface potential was $\psi_s = 0.5$ V, while $a = 0.66$ nm.

Note that the electrolyte relative permittivity and the Stern layer thickness (or solvated ion radius) could be adjusted arbitrarily in order to achieve good agreement between Helmholtz model and experimental data as performed in refs 37–39. However, the effects of electrolyte concentration and electrode potential cannot be predicted explicitly by this approach. In other words, such an approach lacks rigor and thus cannot be used for the systematic optimization of EDLCs.

Overall, the total capacitance $C_s = 31\text{--}37$ $\mu\text{F}/\text{cm}^2$ was about half that predicted assuming constant permittivity (Figure 5). It was dominated by the Stern layer capacitance, as shown in Figure 6. This is consistent with the hypothesis typically made for concentrated electrolyte solutions.^{37–39} Moreover, the electrode curvature had no effect on the predicted specific capacitances C_s^{St} , C_s^{D} , and C_s for sphere radii larger than 40 nm instead of 100 nm when assuming constant permittivity (Figure 5).

In summary, these results demonstrate that the Stern layer as well as the finite ion size and field-dependent electrolyte permittivity needs to be accounted for in simulating EDLCs. This is particularly true when the electrode sphere radius is small and less than 40 nm for aqueous electrolytes.

Note that Hamou et al.²⁸ investigated the effect of field-dependent electrolyte permittivity in the simulation of SECPMs using the Booth model. Unfortunately, the parameters used in the Booth model were not reported in ref 28. Unlike the present study, the authors did not observe significant changes in the dielectric permittivity and in electric potential profiles.²⁸ This may be attributed to the following two reasons. First, the electrolyte concentration and the surface potential considered in ref 28 were $c_\infty = 10^{-5}\text{--}10^{-3}$ mol/L and $\psi_s = 0.2\text{--}0.4$ V. These values were lower than $c_\infty = 1$ mol/L and $\psi_s = 0.5$ V used in the present study. Second, electric double layers between the working electrode and the probe overlapped in the simulations of SECPMs.²⁸ This could significantly reduce the local electric field making the dependency of the electrolyte permittivity on the electric field negligible.⁷⁰

4.4. Effect of Stern Layer Thickness. Figure 7 shows the diffuse layer specific capacitance C_s^D as a function of R_0 obtained by solving eqs 11a, 11b, and 12a–12c using field-dependent permittivity for Stern layer thickness $H = 0$, 0.33, and 1.0 nm. The case of $H = 0$ nm corresponds to the simulation of the diffuse

layer without Stern layer. The other parameters were identical to those used to produce Figure 6. Figure 7 shows that C_s^D decreased with decreasing Stern layer thickness for all values of particle radius R_0 . The predicted C_s^D significantly decreased with increasing sphere radius R_0 for finite Stern layer thickness H . However, in the limiting case of $H = 0$ nm (i.e., without Stern layer), C_s^D remained nearly independent of R_0 .

5. CONCLUSION

This paper presented numerical simulations of the electric double layer near the surface of a spherical ultramicroelectrode particle immersed in aqueous electrolyte solution. The model accounted for (i) the Stern and diffuse layers, (ii) the finite size of ions in both layers, and (iii) the field-dependent electrolyte permittivity. The effect of electrode curvature was also investigated by varying the particle radius from 1 nm to 100 μm . The following conclusions can be drawn:

1. The field-dependent permittivity $\epsilon_r(E)$ significantly affects predictions of the Stern layer and total specific capacitances for all particle radii considered.
2. The finite size of ions and the Stern layer need to be accounted for in predicting the electric double layer capacitance for large electric potential (~ 0.5 V) and electrolyte concentration (~ 1 mol/L).
3. The electrode curvature has negligible effect on the Stern layer and diffuse layer specific capacitances for sphere radii larger than 40 nm for both constant and field-dependent permittivities.
4. The Stern layer capacitance dominates the total capacitance when the electrolyte concentration and surface potential are large ($c_\infty \geq 1$ mol/L and $\psi_s \geq 0.5$ V).
5. The Helmholtz model predicts the Stern layer capacitance C_s^{St} of a sphere if the electrolyte permittivity can be assumed to be constant or if the sphere radius is larger than 40 nm.
6. The Helmholtz model significantly underestimates C_s^{St} for sphere radii less than 40 nm when accounting for field-dependent permittivity.

These conclusions will be useful in accurately simulating ultramicroelectrodes for electrochemical sensors and EDLCs with more complex geometries.

AUTHOR INFORMATION

Corresponding Author

*Phone: (310) 206-5598. Fax: (310) 206-2302. E-mail: pilon@seas.ucla.edu.

ACKNOWLEDGMENT

This material is based upon work supported as part of the Molecularly Engineered Energy Materials, an Energy Frontier Research Center funded by the U.S. Department of Energy, Office of Science, Office of Basic Energy Sciences, under Award No. DE-SC0001342.

REFERENCES

- (1) Wightman, R. Voltammetry with microscopic electrodes in new domains. *Science* **1988**, *240*, 415–420.
- (2) Penner, R.; Heben, M.; Longin, T.; Lewis, N. Fabrication and use of nanometer-sized electrodes in electrochemistry. *Science* **1990**, *250*, 1118–1121.

- (3) Heinze, J. Ultramicroelectrodes in electrochemistry. *Angew. Chem., Int. Ed.* **1993**, *32*, 1268–1288.
- (4) Aoki, K. Theory of ultramicroelectrodes. *Electroanalysis* **1993**, *5*, 627–639.
- (5) Stulik, K.; Amatore, C.; Holub, K.; Marecek, V.; Kutner, W. Microelectrodes. definitions, characterization, and applications (technical report). *Pure Appl. Chem.* **2000**, *72*, 1483–1492.
- (6) Arrigan, D. Nanoelectrodes, nanoelectrode arrays and their applications. *Analyst* **2004**, *129*, 1157–1165.
- (7) Shao, Y.; Mirkin, M.; Fish, G.; Kokotov, S.; Palanker, D.; Lewis, A. Nanometer-sized electrochemical sensors. *Anal. Chem.* **1997**, *69*, 1627–1634.
- (8) Murray, R. Nanoelectrochemistry: Metal nanoparticles, nanoelectrodes, and nanopores. *Chem. Rev.* **2008**, *108*, 2688–2720.
- (9) Belding, S.; Campbell, F.; Dickinson, E.; Compton, R. Nanoparticle-modified electrodes. *Phys. Chem. Chem. Phys.* **2010**, *12*, 11208–11221.
- (10) Arico, A.; Bruce, P.; Scrosati, B.; Tarascon, J.-M.; Schalkwijk, W. Nanostructured materials for advanced energy conversion and storage devices. *Nat. Mater.* **2005**, *4*, 366–377.
- (11) Guo, Y.-G.; Hu, J.-S.; Wan, L.-J. Nanostructured materials for electrochemical energy conversion and storage devices. *Adv. Mater.* **2008**, *20*, 2878–2887.
- (12) Balaya, P. Size effects and nanostructured materials for energy applications. *Energy Environ. Sci.* **2008**, *1*, 645–654.
- (13) Manthiram, A.; Murugan, A.; Sarkar, A.; Muraliganth, T. Nanostructured electrode materials for electrochemical energy storage and conversion. *Energy Environ. Sci.* **2008**, *1*, 621–638.
- (14) Whittingham, M. Materials challenges facing electrical energy storage. *MRS Bull.* **2008**, *33*, 411–419.
- (15) Simon, P.; Gogotsi, Y. Materials for electrochemical capacitors. *Nat. Mater.* **2008**, *7*, 845–854.
- (16) Liu, J.; Cao, G.; Yang, Z.; Wang, D.; Dubois, D.; Zhou, X.; Graff, G.; Pederson, L.; Zhang, J.-G. Oriented nanostructures for energy conversion and storage. *ChemSusChem* **2008**, *1*, 676–697.
- (17) Su, D.; Schlogl, R. Nanostructured carbon and carbon nanocomposites for electrochemical energy storage applications. *ChemSusChem* **2010**, *3*, 136–168.
- (18) Liu, C.; Li, F.; Ma, L.-P.; Cheng, H.-M. Advanced materials for energy storage. *Adv. Mater.* **2010**, *22*, 28–62.
- (19) Wang, J.; Polleux, J.; Lim, J.; Dunn, B. Pseudocapacitive contributions to electrochemical energy storage in TiO₂ (Anatase) nanoparticles. *J. Phys. Chem. C* **2007**, *111*, 14925–14931.
- (20) Wallace, G.; Chen, J.; Mozer, A.; Forsyth, M.; MacFarlane, D.; Wang, C. Nanoelectrodes: energy conversion and storage. *Mater. Today* **2009**, *12*, 20–27.
- (21) Rolison, D.; Long, J.; Lytle, J.; Fischer, A.; Rhodes, C.; McEvoy, T.; Bourg, M.; Lubers, A. Multifunctional 3D nanoarchitectures for energy storage and conversion. *Chem. Soc. Rev.* **2009**, *38*, 226–252.
- (22) Kalinin, S.; Balke, N. Local electrochemical functionality in energy storage materials and devices by scanning probe microscopies: Status and perspectives. *Adv. Mater.* **2010**, *22*, 193–209.
- (23) Pust, S.; Salomo, M.; Oesterschulze, E.; Wittstock, G. Influence of electrode size and geometry on electrochemical experiments with combined SECM-AFM probes. *Nanotechnology* **2010**, *21*, No. 105709.
- (24) Li, C.; Kjoller, K. (Veeco Instrument Inc.). Scanning Electrochemical Potential Microscopy. U.S. Patent 7,156,965 B1, 2007.
- (25) Hurth, C.; Li, C.; Bard, A. Direct probing of electrical double layers by scanning electrochemical potential microscopy. *J. Phys. Chem. C* **2007**, *111*, 4620–4627.
- (26) Baier, C.; Stimmin, U. Imaging single enzyme molecules under in situ conditions. *Angew. Chem., Int. Ed.* **2009**, *48*, 5542–5544.
- (27) Hamou, R.; Biedermann, P.; Erbe, A.; Rohwerder, M. Numerical analysis of Debye screening effect in electrode surface potential mapping by scanning electrochemical potential microscopy. *Electrochem. Commun.* **2010**, *12*, 1391–1394.
- (28) Hamou, R.; Biedermann, P.; Erbe, A.; Rohwerder, M. Numerical simulation of probing the electric double layer by scanning electrochemical potential microscopy. *Electrochim. Acta* **2010**, *55*, 5210–5222.
- (29) Pech, D.; Brunet, M.; Durou, H.; Huang, P.; Mochalin, V.; Gogotsi, Y.; Taberna, P.-L.; Simon, P. Ultrahigh-power micrometre-sized supercapacitors based on onion-like carbon. *Nat. Nanotechnol.* **2010**, *5*, 651–654.
- (30) von Helmholtz, H. Studien über elektrische grenzschichten. *Ann. Phys.* **1879**, *243*, 337–382.
- (31) Bard, A.; Faulkner, L. *Electrochemical Methods: Fundamentals and Applications*; John Wiley & Sons: New York, 2001.
- (32) Bagotsky, V. *Fundamentals of Electrochemistry*, 2nd ed.; John Wiley & Sons: New York, 2006.
- (33) Butt, H.-J.; Kappl, M. *Surface and Interfacial Forces*; Wiley-VCH: Weinheim, Germany, 2010.
- (34) Masliyah, J.; Bhattacharjee, S. *Electrokinetic and Colloid Transport Phenomena*; John Wiley & Sons: New York, 2006.
- (35) Young, H.; Freedman, R.; Ford, L. *University Physics with Modern Physics*, 12th ed.; Pearson Education: Upper Saddle River, NJ, USA, 2007.
- (36) Halliday, D.; Resnick, R.; Walker, J. *Fundamentals of Physics*, 9th ed.; John Wiley & Sons: New York, 2010.
- (37) Huang, J.; Sumpter, B.; Meunier, V. Theoretical model for nanoporous carbon supercapacitors. *Angew. Chem., Int. Ed.* **2008**, *47*, 520–524.
- (38) Huang, J.; Sumpter, B.; Meunier, V. A universal model for nanoporous carbon supercapacitors applicable to diverse pore regimes, carbon materials, and electrolytes. *Chem.—Eur. J.* **2008**, *14*, 6614–6626.
- (39) Huang, J.; Sumpter, B.; Meunier, V.; Yushin, G.; Portet, C.; Gogotsi, Y. Curvature effects in carbon nanomaterials: Exohedral versus endohedral supercapacitors. *J. Mater. Res.* **2010**, *25*, 1525–1531.
- (40) Gouy, G. Constitution of the electric charge at the surface of an electrolyte. *J. Phys. Theor. Appl.* **1910**, *9*, 457–468.
- (41) Chapman, D. A contribution to the theory of electrocapillarity. *Philos. Mag., Ser. 6* **1913**, *25*, 475–481.
- (42) Hunter, R. *Foundations of Colloid Science*, 2nd ed.; Oxford University Press: New York, 2001.
- (43) Lyklema, J. *Fundamentals of Interface and Colloid Science*; Academic Press: New York, 2001; Vol. 2.
- (44) Ohshima, H. *Theory of Colloid and Interfacial Electric Phenomena*; Academic Press: New York, 2006.
- (45) Stern, O. The theory of the electrolytic double layer. *Z. Elektrochem. Angew. Phys. Chem.* **1924**, *30*, 508–516.
- (46) Torrie, G.; Valleau, J. The electrical double layer. III. Modified Gouy-Chapman theory with unequal ion sizes. *J. Chem. Phys.* **1982**, *76*, 4623–4630.
- (47) Huang, J.; Qiao, R.; Sumpter, B.; Meunier, V. Effect of diffuse layer and pore shapes in mesoporous carbon supercapacitors. *J. Mater. Res.* **2010**, *25*, 1469–1475.
- (48) Kilic, M.; Bazant, M.; Ajdari, A. Steric effects in the dynamics of electrolytes at large applied voltages. I. Double-layer charging. *Phys. Rev. E* **2007**, *75*, No. 021502.
- (49) Bazant, M.; Kilic, M.; Storey, B.; Ajdari, A. Towards an understanding of induced-charge electrokinetics at large applied voltages in concentrated solutions. *Adv. Colloid Interface Sci.* **2009**, *152*, 48–88.
- (50) Outhwaite, C.; Bhuiyan, L. An improved modified Poisson-Boltzmann equation in electric-double-layer theory. *J. Chem. Soc., Faraday Trans. 2* **1983**, *79*, 707–718.
- (51) Vlachy, V. Ionic effects beyond Poisson-Boltzmann theory. *Annu. Rev. Phys. Chem.* **1999**, *50*, 145–165.
- (52) Kornyshev, A. Double-layer in ionic liquids: Paradigm change? *J. Phys. Chem. B* **2007**, *111*, 5545–5557.
- (53) Biesheuvel, P.; van Soestbergen, M. Counterion volume effects in mixed electrical double layers. *J. Colloid Interface Sci.* **2007**, *316*, 490–499.
- (54) Bikerman, J. Structure and capacity of electrical double layer. *Philos. Mag.* **1942**, *33*, 384–397.
- (55) Borukhov, I.; Andelman, D.; Orland, H. Steric effects in electrolytes: A modified Poisson-Boltzmann equation. *Phys. Rev. Lett.* **1997**, *79*, 435–438.
- (56) Dickinson, E.; Compton, R. Diffuse double layer at nanoelectrodes. *J. Phys. Chem. C* **2009**, *113*, 17585–17589.

(57) Henstridge, M.; Dickinson, E.; Compton, R. On the estimation of the diffuse double layer of carbon nanotubes using classical theory: Curvature effects on the Gouy-Chapman limit. *Chem. Phys. Lett.* **2010**, *485*, 167–170.

(58) Booth, F. The dielectric constant of water and the saturation effect. *J. Chem. Phys.* **1951**, *19*, 391–394.

(59) Booth, F. Dielectric constant of polar liquids at high field strengths. *J. Chem. Phys.* **1955**, *23*, 453–457.

(60) Appleby, A. Electron transfer reactions with and without ion transfer. *Modern Aspects of Electrochemistry*; Conway, B., Vayenas, C., White, R., Gamboa-Adelco, M., Eds.; Kluwer Academic/Plenum Publishers: New York, 2005; No. 38; pp 175–301.

(61) Buckingham, A. Theory of the dielectric constant at high field strengths. *J. Chem. Phys.* **1956**, *25*, 428.

(62) Yeh, I.-C.; Berkowitz, M. Dielectric constant of water at high electric fields: Molecular dynamics study. *J. Chem. Phys.* **1999**, *110*, 7935.

(63) Fulton, R. The nonlinear dielectric behavior of water: Comparisons of various approaches to the nonlinear dielectric increment. *J. Chem. Phys.* **2009**, *130*, No. 204503.

(64) Yang, L.; Fishbine, B.; Migliori, A.; Pratt, L. Dielectric saturation of liquid propylene carbonate in electrical energy storage applications. *J. Chem. Phys.* **2010**, *132*, No. 044701.

(65) Zarzycki, P.; Rosso, K. Molecular dynamics simulation of the AgCl/electrolyte interfacial capacity. *J. Phys. Chem. C* **2010**, *114*, 10019–10026.

(66) Conway, B. *Electrochemical Supercapacitors: Scientific Fundamentals and Technological Applications*; Kluwer Academic/Plenum Publishers: New York, 1999.

(67) Gur, Y.; Ravina, I.; Babchin, A. On the electrical double layer theory. II. The Poisson-Boltzmann equation including hydration forces. *J. Colloid Interface Sci.* **1978**, *64*, 333–341.

(68) Basu, S.; Sharma, M. Effect of dielectric saturation on disjoining pressure in thin films of aqueous electrolytes. *J. Colloid Interface Sci.* **1994**, *165*, 355–366.

(69) Paunov, V.; Dimova, R.; Kralchevsky, P.; Broze, G.; Mehreteab, A. The hydration repulsion between charged surfaces as an interplay of volume exclusion and dielectric saturation effects. *J. Colloid Interface Sci.* **1996**, *182*, 239–248.

(70) Wang, H.; Varghese, J.; Pilon, L. Simulation of electric double layer capacitors with mesoporous electrodes: Effects of morphology and electrolyte permittivity. *Electrochim. Acta* **2011**, *56*, 6189–6197.

(71) Israelachvili, J. N. *Intermolecular and Surface Forces*, 3rd ed.; Academic Press: New York, 2010.

(72) Griffiths, D. *Introduction to Electrodynamics*, 3rd ed.; Prentice Hall: New York, 1999.

(73) Feynman, R.; Leighton, R.; Sands, M. *The Feynman Lectures on Physics*, 2nd ed.; Addison-Wesley: Reading, MA, USA, 2005; Vol. 2.